Acta Astronautica 212 (2023) 624–629

Contents lists available at ScienceDirect

Acta Astronautica

journal homepage: www.elsevier.com/locate/actaastro

Satellite uplink interference measurements in the 437 MHz UHF amateur radio band onboard LUME-1

Gara Quintana-Diaz [a,1], Torbjörn Ekman [a], Alejandro Camanzo [b], Roger Birkeland [a,*], José Miguel Lago [c], Alberto González Muíño [d], Fernando Aguado Agelet [b,a]

[a] Department of Electronic Systems, Norwegian University of Science and Technology (NTNU), O.S. Bragstads plass 2b, 7034 Trondheim, Norway
[b] atlanTTic Research center, Aerospace Technology Group, Escola de Enxeñaría de Telecomunicación, University of Vigo, Spain
[c] Escola de Enxeñaría de Telecomunicación, University of Vigo, Vigo, Spain
[d] Alén Space, Nigrán, Spain

ARTICLE INFO

Keywords:
Amateur radio band
Interference statistics
In-orbit measurements
Small satellite
UHF

ABSTRACT

Satellite operators struggle to communicate with their satellites over Europe in the UHF amateur band (430–440 MHz) due to high power in-orbit interference. Statistical characterisation of the interference beyond average interference levels using in-orbit measurements is useful for the design of suitable countermeasures. Some recent studies have started to investigate both the frequency and time behaviour of the interference, but more measurements are needed to cover the whole UHF amateur band. In this paper, we use the Local Mean Envelope (LME) method to analyse the time and frequency characteristics of in-orbit radio interference from the LUME-1 satellite, measured in the 437 MHz band. Satellite measurements were performed on a TOTEM Software-Defined Radio (SDR), in orbit over Europe and Antarctica and the results were downloaded for analysis on the ground. The average power spectrum and the variability of the LME for different time windows in the 437 MHz band are presented. The data analysis also includes the coefficient of variation of the LME to study the dispersion of the interference. The results are compared to previous measurements in the 435 MHz band using the same method. The new results are found to differ compared with previous measurements on the 435 MHz band. The bandwidth of the band-limited signals measured at 435 MHz was found to be 300 kHz, and at 437 MHz, 200 kHz wide for this dataset. Also, the interference power was found to be higher for 437 MHz. In both cases the interference behaviour is highly non-Gaussian, suggesting that typical communication countermeasures will not be sufficient. Although more measurements are needed for better spatial resolution, our findings may contribute to explaining why satellite operations are difficult on these bands. A better knowledge of the time and frequency variability of the interference can indicate which mitigation techniques are required and are efficient to improve satellite communication in that band.

1. Introduction

The 400–500 MHz UHF band encompasses several bands used for satellite communications, such as the 401–403 MHz Earth Exploration Satellite Service (EESS) or the amateur band from 435 to 438 MHz. The amateur radio band has been a popular choice for university small satellite missions [1] for more than 20 years. However, not all of those missions follow the correct procedure and apply for frequency allocation from the International Telecommunication Union (ITU) [2] properly. This situation, combined with the operations challenges due to poor uplink communication experienced by past and current satellite mission operators [3–6], motivates in-orbit radio measurements to better map the interference environment.

Spectrum monitoring applications and interference analysis have been promoted by the European Space Agency (ESA) in different projects [7–10]. In addition, space spectrum monitoring has become a popular business case for several companies, such as Aurora Insight [11], Umbra [12], HawkEye 360 [13], Kleos Space [14] and Horizon Technologies (Amber) [15].

With a better understanding of the interference environment and the characteristics of the interference, more resilient radio systems can be designed. Since some interference sources cannot be inhibited, satellite

* Corresponding author.
E-mail address: roger.birkeland@ntnu.no (R. Birkeland).
[1] Current affiliation: Space Norway AS, Skøyen, Norway.

https://doi.org/10.1016/j.actaastro.2023.08.010
Received 27 February 2023; Received in revised form 11 May 2023; Accepted 9 August 2023
Available online 12 August 2023

Acronyms/Abbreviations

AWGN	Additive White Gaussian Noise.
CV	coefficient of variation.
DFT	Discrete Fourier Transform.
ECDF	Empirical Cumulative Density Function.
ESA	European Space Agency.
IQ	In-Phase and Quadrature.
ISS	International Space Station.
ITU	International Telecommunication Union.
LME	Local Mean Envelope.
NTNU	Norwegian University of Science and Technology.
SDR	Software-Defined Radio.
TU Berlin	Technische Universität Berlin.
UVigo	University of Vigo.

operators need to learn how to co-exist with the interference and how satellite communication systems can be improved.

In this paper, we present new in-orbit results from measurement campaigns carried out in February and June 2022 as well as in February 2023 with the LUME-1 satellite. The centre frequency is set to 437.28 MHz to cover the LUME-1 operations frequency [16] and the SelfieSat frequency [17]. We also compare the new 170 results with the previous measurements over the same area performed from December 2020 to June 2021 centred at 435 MHz. Furthermore, some measurements over the Antarctic were performed in the 437 MHz band in February 2023 to obtain a noise floor reference.

The following subsection summarises the state-of-the-art of in-orbit interference measurements. In Section 2, the LUME-1 satellite is introduced, the measurement algorithm applied is briefly explained and the measurement campaigns are described. The results are explained and discussed in Section 3. Finally, the conclusions are presented in Section 4.

1.1. Related work

The Technische Universität Berlin (TU Berlin), the University of Vigo (UVigo) and the University of Würzburg have performed radio spectrum measurements after experiencing difficulties operating their own satellites [3,4,6]. TU Berlin and UVigo encountered problems operating their satellites LAPAN-TUBSAT and HumSat-D in 2013. UVigo detected strong pulsed interference inhibiting their communications with HumSat-D. Furthermore, University of Würzburg measured high-power interference over central Europe using the UWE-3 satellite. TU Berlin continued performing interference measurements by installing a Software-Defined Radio (SDR) in the International Space Station (ISS) for spectrum monitoring in 2019 and launching the SALSAT satellite one year later [18].

Most of the published results on interference measurements from small satellites in the UHF band focus on the average interference power over a certain measurement duration [6] and do not consider the time structure of the interference. Heatmaps have been a traditional way of showing the average power of interference [4,6], but they do not show the time variability or dispersion of the interference. In this paper, both the time and frequency characteristics of the interference are analysed.

2. Material and methods

In the following subsections, the measurement and analysis methods are explained.

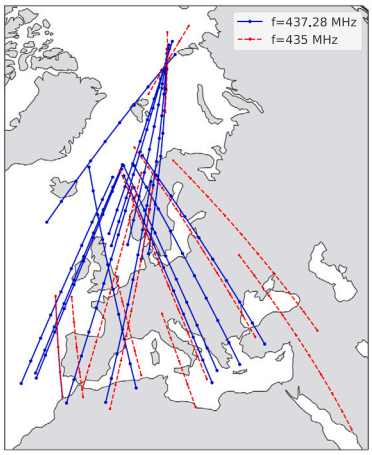

Fig. 1. Measurements tracks centred over Europe. (For interpretation of the references to colour in this figure legend, the reader is referred to the web version of this article.).

2.1. LUME-1

The LUME-1 is a 2U CubeSat developed by UVigo (Spain) that was launched into a polar orbit in 2018. The mission for LUME-1 was to detect and monitor forest fires for the Fire RS European project [19]. Since that mission ended in June 2019, the satellite was available for other research. The Norwegian University of Science and Technology (NTNU) is collaborating with UVigo, and thus, uses the satellite for in-orbit radio measurements. The satellite measurements are performed with the SDR connected to a turnstile antenna on-board LUME-1 with near omni-directional antenna pattern. The satellite is tumbling and the exact footprint is thus difficult to determine. This will cause minor power fluctuations in the measurements that are not easily identifiable and have not been considered in this paper. The frequency band of the SDR is the UHF amateur radio band ranging from 435 MHz to 438 MHz. The measurements discussed in this article have been centred at 437.28 MHz. Both the uplink and the downlink throughput are limited for LUME-1. The estimated net downlink data rate is about 1 kbps, and 200 bps for the uplink. Both links are available for around 5 min a day. The uplink is severely affected by the interference we measure in this paper. Raw measurements of the RF spectrum generate a vast amount of data depending on selected bandwidth, sampling rate and, measurement duration. Due to downlink throughput constraints, the analysis algorithm used onboard must generate a very small data volume, resulting in about 40 kB for a set of ten individual measurements of five seconds each. Onboard processing was performed to achieve this.

2.2. Analysis algorithm

To overcome the limitations of the data throughput and still analyse both the time and frequency characteristics of the interference, the Local Mean Envelope (LME) algorithm was designed [20]. The LME measures the variability over the measurement between local mean envelopes for different averaging window sizes in a region. It measures how long time averages are needed to obtain local means that are close to the ergodic mean, estimated as the mean in that region. The local mean envelopes for non-overlapping widows are considered as stochastic variables. The first and second-order moments for this process will depend on the length of the averaging window and the time variability and distribution of the measured signal. When the length of the averaging windows increases, the local mean envelope will approach the mean envelope in that region. The measured signal is considered to be stationary in the mean (first-order stationarity) for

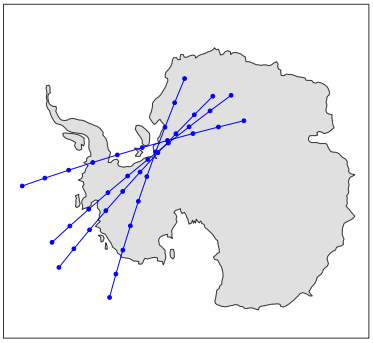

Fig. 2. Measurements tracks over the Antarctic.

time intervals long enough to obtain local means that does not vary significantly in that region.

The LME algorithm is implemented on the In-Phase and Quadrature (IQ) samples acquired by the SDR and continuous Discrete Fourier Transforms (DFTs) are applied with no overlap during the measurement period. The overall mean and the average power of each frequency bin are calculated. The average power in a region can be used to plot heatmaps. Furthermore, the local mean envelope for time windows of different lengths for every frequency bin allows for time variability analysis. The first-order stationarity window can be estimated using the CV, defined as the ratio between standard deviation of the envelope and the mean envelope. A high CV indicates a disperse envelope. A continuous constant envelop signal has a CV of zero, whereas a complex Gaussian noise has an envelope CV of roughly 0.52. High CV can be obtained from disperse signals as e.g. square pulsed signals with low duty cycles. Here, a duty cycle of 10% results in a CV of 3 and 1% in a CV close to 10.

2.3. Measurement campaigns

The areas of interest considered in this paper are parts of Europe, with a particular focus on Vigo (Spain) and Trondheim (Norway), in addition to Antarctica for low interference (also referred to as noise floor) reference measurements. Three measurement campaigns were performed during 13th–18th February 2022, 25th–27th June 2022 and 1st–3rd February 2023. The satellite ground tracks during measurements over Europe are shown in Fig. 1. The blue tracks are the new measurements centred at 437.28 MHz (February–June 2022 and February 2023) and the red tracks belong to the measurements centred at 435 MHz (spring 2021) and analysed in [20]. Ground tracks for Antarctica are shown in Fig. 2. In both cases, each circle represents one individual measurement that lasts for five seconds.

The configuration of the measurements is shown in Table 2 and the start time of each pass (UTC) is given in Table 1.

3. Results and discussion

To get an overview of the frequency and time variability of the interference, the percentiles of the average power spectra and the coefficient of variation are shown in Fig. 3 for both centre frequencies. The power spectra are averaged over 5 s and in every pass, the individual measurements are occurring every minute. The absolute power values have not been calibrated so the numbers shown are relative values. The CV is defined in [20] and it gives an indication of the spread in magnitude.

The 50% (median) and 90% power spectra percentiles are about 7 dB higher in the 437 MHz band as compared to the 435 MHz band. However, the 10% percentile is 4 dB lower. The cause for the asymmetry is not known yet and more measurements are desirable.

Table 1
UTC times for each pass.

Index	Date	Start time (UTC)
577	2022–02–13	23:28
588	2022–02–17	10:21
589	2022–02–17	23:20
597	2022–02–14	08:34
600	2022–02–14	22:56
602	2022–02–15	08:09
605	2022–02–15	22:31
607	2022–02–16	07:44
609	2022–02–16	22:06
616	2022–02–18	08:27
619	2022–02–18	22:49
624	2022–06–25	23:09
626	2022–06–26	22:42
629	2022–06–27	22:14
645	2022–06–27	09:21
657	2023–02–01	21:50
668	2023–02–03	23:49
690	2023–02–02	18:53
691	2023–02–02	20:26
699	2023–02–03	16:46
700	2023–02–03	18:19

Table 2
Measurement configuration.

Parameter	Value
Centre frequency (MHz)	437.28
Bandwidth (kHz)	500[a]
Number of frequency bins	128
Frequency resolution (kHz/bin)	4.8

[a]The bandwidth was configured to 200 kHz but the 3 dB bandwidth is larger [20].

A band-limited signal appears in all cases and is in the centre of the band, except for the 10% percentile at 437.28 MHz. In Fig. 3(a) the bandwidth of this signal is 300 kHz and in the 50% and 90% percentile of Fig. 3(b) the bandwidth is 200 kHz. The 300 kHz interference signal appears in all the percentiles of the 435 MHz measurements.

The coefficient of variation, which measures the spread in the average envelope, is also higher for the 437.28 MHz case. Within the SDR bandwidth marked by the vertical black dotted lines, the CV is higher where the band-limited interference signal can be seen in the average power spectra plots. High power and high CV indicate that there are strong signals with a high spread in magnitude. A high CV is often the result of repeated short bursts of high power [21]. Fig. 3(c) also shows that the signals measured do not follow an Additive White Gaussian Noise (AWGN) behaviour. Thus, applying countermeasures and estimating link budgets assuming AWGN will not be useful in this environment.

The time variability of the north-to-south passes in Europe and the high north has been analysed in Fig. 4. The average power spectra have been integrated over the 500 kHz bandwidth and plotted with time. The measurement tracks are from north-to-south and the time between measurement points is one minute. The variation of the integrated power over the bandwidth for the northern passes is shown in Fig. 4(c). The power values of the different measurements follow a similar trend, increasing 12 dB as the satellite moves from north to south. The power levels measured over the high north are similar to the levels in the southern part of the tracks in Fig. 4(d).

In Fig. 4(d), all the tracks over Western Europe show a similar tendency in integrated power. The values of the red and blue passes over Western Europe are more similar since they are closer to each other. As the tracks move to the east, the power drop is delayed. There is higher power when the satellite is over central Europe.

To get an overview of the spatial power variation, the measurements points at 437.28 MHz in Fig. 1 that are between −35° to 35° in longitude have been divided into regions in Fig. 5(a), similarly to in [20].

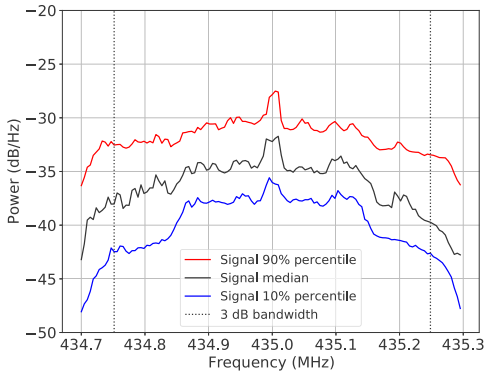

(a) Average power spectra percentiles centered at 435 MHz.

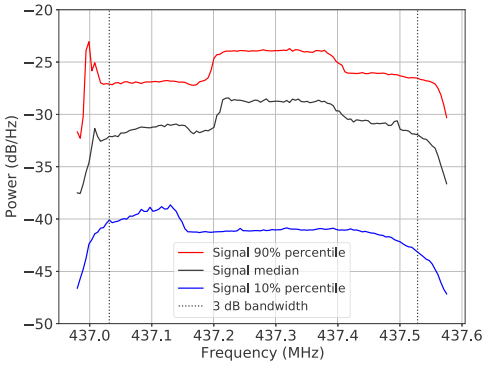

(b) Average power spectra percentiles centered at 437.28 MHz.

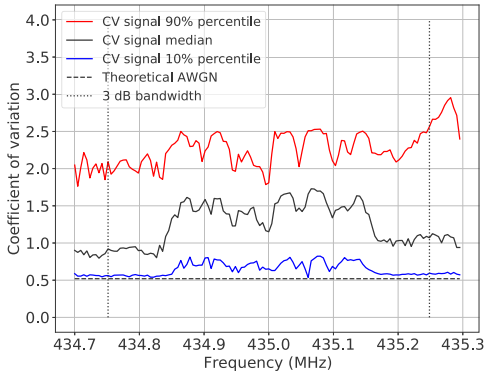

(c) Coefficient of variation percentiles centered at 435 MHz.

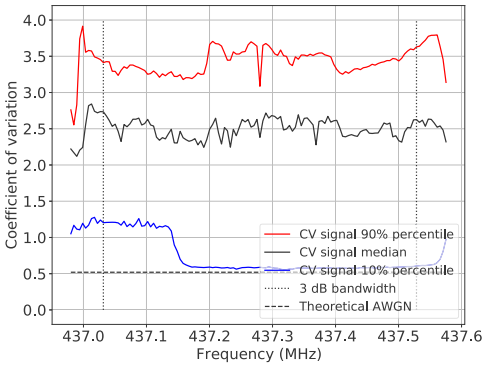

(d) Coefficient of variation percentiles centered at 437.28 MHz.

Fig. 3. Time and frequency statistics. A high spread in the average envelope corresponds to a high CV.

The Empirical Cumulative Density Functions (ECDFs) of average power during each 5 s measurement including all frequency bins within the bandwidth are shown in Fig. 5(b). The colours of the measurement points in the map correspond to those in the ECDFs.

The black dotted line in Fig. 5(b) corresponds to the measurements over the Antarctic. Since the ECDF shows power levels considerably lower than the rest because the area is less populated, it is considered the noise floor of the band. It should be noted that there is some activity in the Antarctic due to research bases, and some of them are within our measurement footprint for part of a pass (c.f. Fig. 2), but it is clear from the results that the power levels (c.f. Fig. 5(b)) are much lower compared to more populated areas.

Regarding the populated areas, about 80% of the measurement points over 75° latitude and those in the southwest corner have power levels 13 dB lower than in central Europe. The region between 60°–75° has about 5 dB less power than central Europe for 80% of the points. These results help explain the difficulties experienced by small satellite operators from universities located in central Europe, including UVigo (Spain). This university is located in the north-west of Spain where the interference power behaviour changes from region $R1$ to $R2$.

The window of stationarity of the first-order was estimated using the LME method and the CV for each time window as described in [20]. In Fig. 6, the time variability of the measurements centred at 435 MHz and the ones at 437.28 MHz is compared both within the band-limited signal bandwidth and outside. For the 435 MHz case, the observed band-limited signal bandwidth was 300 kHz, and for the 437.28 MHz, the same parameter was found to be 200 kHz. The percentage of measurements with a stationarity window longer than 27.3 ms is higher for the new measurements at 437.28 MHz both within the bandwidth of the band-limited signal (solid-filled bars) and outside (patterned bars). It is at almost 70% compared to the 43% (within) and 30% (outside) of the 435 MHz measurements. These results indicate that the interference has a high time variability and most measurements do not show a stationary behaviour in windows shorter than 27.3 ms. Thus, to be able to estimate interference statistics the time window to be used should be at least longer than 30 ms because there is too much time variability in lower time scales.

4. Conclusions

We have presented time and frequency measurement results of in-orbit radio interference from the LUME-1 satellite recorded in 2022 and 2023. The results of 210 individual 500 kHz bandwidth measurements in the 437 MHz band over Europe are compared to previous measurements in the 435 MHz band, also within the UHF amateur band.

The average interference power and the spread in envelope were higher in the 437.28 MHz band than in the 435 MHz band, explaining the challenges experienced by the small satellite operators. A 200 kHz band-limited interference signal was detected in the new measurements centred at 437.28 MHz in contrast with the 300 kHz bandwidth of the signal at 435 MHz. The interference behaviour is highly non-Gaussian, so countermeasures, such as error correction codes, and link budgets that assume AWGN will not be realistic in this band.

Building interference statistics requires many measurements to gather the long-term time variability. These statistics can be useful in designing or improving existing satellite communication systems.

Declaration of competing interest

The authors declare that they have no known competing financial interests or personal relationships that could have appeared to influence the work reported in this paper.

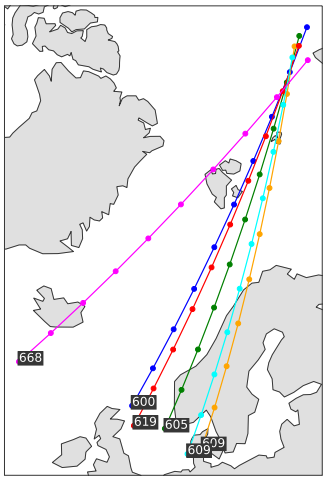

(a) Measurement passes over the high north and Scandinavia.

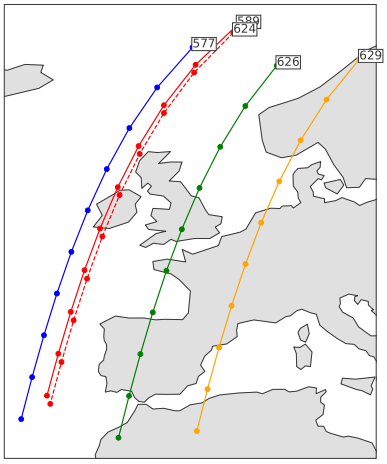

(b) Measurement passes in the west of Europe.

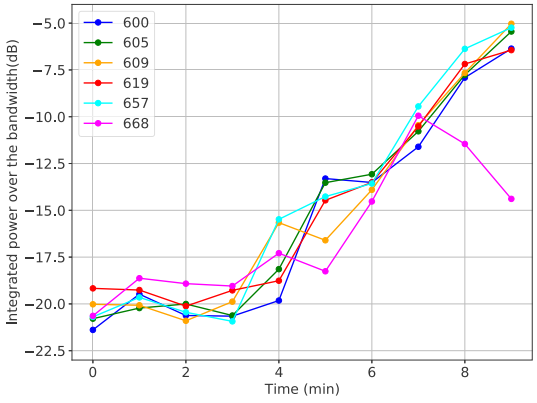

(c) Integrated power over bandwidth for passes over the high north and Scandinavia.

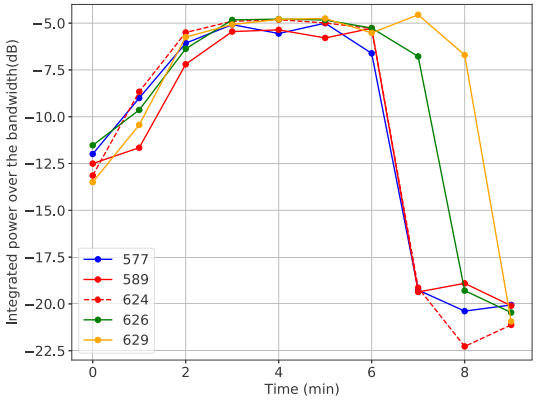

(d) Integrated power over the bandwidth for passes in the west of Europe.

Fig. 4. Integrated power over bandwidth for north–south passes in Europe and the high north centred at 437.28 MHz. (For interpretation of the references to colour in this figure legend, the reader is referred to the web version of this article.)

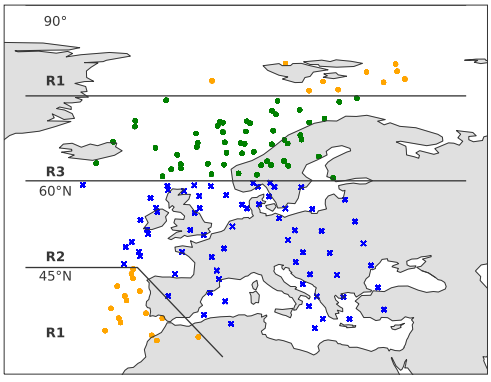

(a) Measurement positions divided into three regions.

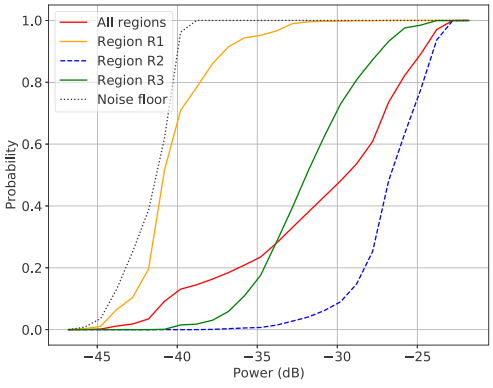

(b) Empirical Cumulative Density Function (ECDF) of average power over the three regions. All frequency bins have been included in the estimation.

Fig. 5. Distribution of average power over Europe and the high north.

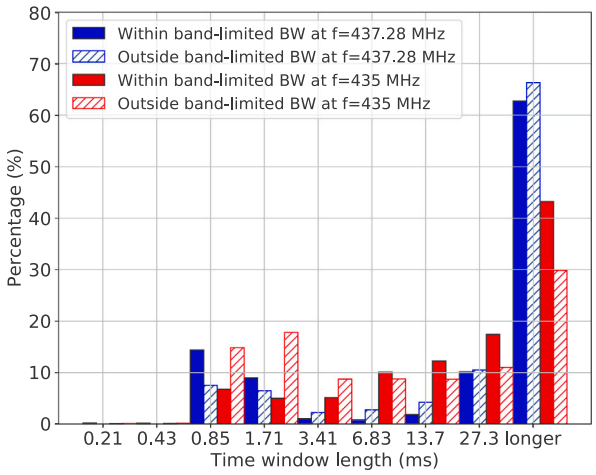

Fig. 6. Stationarity window histogram comparing the measurements centred at 435 MHz and 437.28 MHz. The histogram time window lengths are multiples of one FFT length.

Acknowledgements

This article is an extended version based on a paper presented at the International Astronautical Congress in Paris 2022. The work of the Norwegian University of Science and Technology (NTNU) is supported by the Norwegian Research Council (Grant No. 270959), the Norwegian Space Agency, and the Centre of Autonomous Marine Operations and Systems (NTNU AMOS), Norway. The work of UVigo is supported by Ministerio de Ciencia e Innovación in Spain (Grant No. ESP2016-79184-R).

References

[1] ITU-R: Report ITU-R. SA.2312-0, Characteristics, Definitions and Spectrum Requirements of Nanosatellites and Picosatellites, as Well as Systems Composed of Such Satellites, Tech. rep., ITU, 2014.

[2] ITU-R: Report ITU-R SA.2348-0, Current Practice and Procedures for Notifying Space Networks Currently Applicable to Nanosatellites and Picosatellites, Tech. rep., ITU, 2015.

[3] F. Aguado Agelet, D. Nodar López, A. González Muiño, Preliminary noise measurements campaign carried out by HUMSAT-D during 2014, in: ITU Conference and Workshop on the Small Satellite Regulation and Communication Systems, 2015, pp. 1–21.

[4] S. Busch, et al., UWE-3, in-orbit performance and lessons learned of a modular and flexible satellite bus for future pico-satellites, Acta Astronaut. 117 (2015) 73–89, http://dx.doi.org/10.1016/j.actaastro.2015.08.002.

[5] G. Quintana-Diaz, et al., Detection of radio interference in the UHF amateur radio band with the serpens satellite, Adv. Space Res. 69 (2) (2022) 1159–1169, http://dx.doi.org/10.1016/j.asr.2021.10.017, URL https://www.sciencedirect.com/science/article/pii/S0273117721007778.

[6] M. Buscher, Investigations on the Current and Future Use of Radio Frequency Allocations for Small Satellite Operations, Vol. 7, Universitätsverlag der TU Berlin, 2019.

[7] European Space Agency (ESA), ESA artes frequency monitoring, 2016, https://artes.esa.int/projects/board-spectrum-monitoring-obsm.

[8] European Space Agency, On-board interference geo-location system (ARTES 5.1 5A.037) , 2016, https://artes.esa.int/funding/onboard-interference-geolocation-system-artes-51-5a037-0.

[9] European Space Agency (ESA), Spectrum monitoring mission feasibility assessment(ARTES FPE 1B.129), 2016, https://artes.esa.int/funding/spectrum-monitoring-mission-feasibility-assessment-artes-fpe-1b129.

[10] European Space Agency, Radio frequency analytics applications (ARTES), 2021, https://business.esa.int/funding/call-for-proposals-artes-satcom-apps/radio-frequency-analytics-applications.

[11] Aurora Insight Inc., Aurora Insight, https://aurorainsight.com/.

[12] Iluminate the world | umbra, 2021, https://umbra.space/. (Accessed on 22 Dec 2021).

[13] K. Sarda, et al., Making the invisible visible: Precision RF-emitter geolocation from space by the HawkEye 360 pathfinder mission, in: Proceedings of the 32nd Annual AIAA/USU Conference on Small Satellites, "Logan UT, USA", 2018.

[14] Space powered signal & geospatial intelligence | Kleos, 2021, https://kleos.space/. (Accessed on 22 Dec 2021).

[15] Amber space-based maritime domain intelligence solutions | horizon technologies, 2021, https://horizontechnologies.eu/products/cubesat/. (Accessed on 22 Dec 2021).

[16] University of Vigo- LUME-1 satellite. Telemetry modulation, codes and format, University of Vigo, http://fire-rs.com/static/pdf/LUME-TMandBeacons-1.4-20190107_4.pdf.

[17] Orbit NTNU- Selfie Sat, Orbit NTNU, https://orbitntnu.com/selfiesat/.

[18] J. Freymuth, et al., SALSAT: First mission results of the global RF spectrum analysis in the VHF, UHF and space research bands measured by the spectrum analysis SATellite, in: 73Rd International Astronautical Congress, IAC, 2022.

[19] F. Pérez-Lissi, et al., FIRE-RS: Integrating land sensors, cubesat communications, unmanned aerial vehicles and a situation assessment software for wildland fire characterization and mapping, in: 69th International Astronautical Congress, 2018.

[20] G. Quintana-Diaz, et al., In-orbit measurements and analysis of radio interference in the UHF amateur radio band from the LUME-1 satellite, Remote Sens. 13 (16) (2021) http://dx.doi.org/10.3390/rs13163252, URL https://www.mdpi.com/2072-4292/13/16/3252.

[21] G. Quintana-Díaz, et al., In-orbit interference measurements and analysis in the VDES-band with the NorSat-2 satellite, in: 2022 IEEE Aerospace Conference, AERO, 2022, pp. 1–8, http://dx.doi.org/10.1109/AERO53065.2022.9843810.